Annular Modes in a Multiple Migrating Zonal Jet Regime

Cegeon J. Chan, Ivana Cerovecki, and R. Alan Plumb

May 1, 2006

Program of Atmospheres, Oceans, and Climate, Department of

Earth, Atmospheric and Planetary Sciences,

Massachusetts Institute of Technology, Cambridge, Massachusetts

Corresponding address: Cegeon Chan, Department of Earth and Atmospheric Science,

MIT Building 54, Room 1719, 77 Massachusetts Avenue, Cambridge, MA, 02139

E-mail: cegeon@mit.edu

Abstract

We investigate the dynamics of migrating jets using the MITGCM. The forcings imposed in the model are an idealized atmospheric wind stress and relaxation to a latitudinal temperature profile held constant in time. While the model output shows striking similarities to the observed atmospheric annular modes, where the leading mode of variability is associated with the primary zonal jet's meridional undulation, secondary (weaker) jets emerge and systematically migrate equatorward.

As a result of the propensity for Rossby waves to propagate equatorward on a sphere, the peak of the eddy forcing occurs on the equatorward flanks of the jets, furthering its migration. Besides spherical geometric effects, we will discuss other necessary conditions for jet migration.

1 Introduction

Multiple zonal jets have been observed in various geophysical fluids such as the Earth's ocean (e.g. Roden 2000) and Jovian atmospheres (e.g. Pater and Lissauer 2001). Such behavior is predicted by the theory of β-plane turbulence (Rhines 1975) when the Burger number, $Bu \equiv (\frac{L_D}{L})^2$ is small, where L_D is the deformation radius and L is the length scale of the forcing. A range of modelling studies have been conducted. A two-layer quasi-geostrophic beta-plane (Panetta 1993), barotropic (e.g. Williams 1978), shallow water (e.g. Cho and Polvani 1996) and a primitive equation model on a sphere (Lee 2005) have all discussed the parameters needed for multiple jets.

Using a primitive equation model on a sphere with a thin atmospheric layer, such as those seen on Jupiter, Williams (2003) found multiple jets, which under certain conditions migrated systematically equatorward. Because $Bu \ll 1$ in the Earth's ocean, such a setup is analogous to those seen on giant planets. Treguier and Panetta (1994) used a quasi-geostrophic wind-forced channel model to simulate the Antarctic Circumpolar Current; although multiple jets emerged, no migration was evident.

In this paper, we describe migrating jets in a model of a near-hemispheric ocean. The flow comprises a main jet in low latitudes, which "wobbles" quasi-periodically, and secondary jets, which migrate systematically equatorward, similar to the behavior described by Williams (2003). This equatorward migration is in contrast to the poleward propagation observed in the atmosphere (Feldstein 1998). Since the model-imposed forcings are constant in time with flat-bottom topography, internal dynamics must be responsible for establishing the

remarkable persistence of the migrating zonal jets. Therefore, one of the goals of this paper is to determine what features make the secondary jets migrate.

A cursory description of the model and its equilibrated features will be presented in section 2. The spatial and temporal variability will be analyzed in section 3. Description of the eddy properties will be shown in section 4 and its effects on a sphere in section 5. We conclude with a summary of our important findings in section 6.

2 Model Setup

The data in this study were generated by Cerovecki et al. (2006) from the MIT General Circulation Model (cf. Marshall et al. 1997a; Marshall et al. 1997b.) Readers are referred to Cerovecki et al. (2006) for a complete description of the model setup and the equilibrated states. Here, we just provide a cursory description.

This is a zonally reentrant, semi-hemispheric model ranging from 50.67°S to 0.17°S and 0°E to 10° E on a $\frac{1}{6}^\circ \times \frac{1}{6}^\circ$ latitude/longitude grid. The model-imposed forcings include a wind stress and a heat forcing, both of which are a function of latitude only with a length scale one to two orders of magnitude larger than the Rossby radius of deformation. With such a broad forcing, as discussed by Panetta (1993), multiple jets emerge, as shown in Fig. 1. While the primary jet, located between 15°S to 20°S, "wobbles," as discussed in the next section, secondary (weaker) jets emerge and systematically migrate equatorward.

As discussed in Cerovecki et al. (2006), (see their Fig. 7), poleward of 14°S, the isopycnals have significant slopes, and the region is baroclinically unstable. Moreover, poleward of 20°S,

potential vorticity (PV) is homogenized in the near-adiabatic interior. The likely mechanism in smoothing PV can be attributed to eddies transporting PV downgradient (see Rhines and Young 1982; Kuo et al. 2005).

3 Description of Variability

Fig. 2 shows the vertically-integrated, zonally-averaged zonal flow anomalies as a function of latitude and time. The equatorward migration is clearly seen poleward of the primary jet, in particular, between 20°S and 30°S. From the emergence of the secondary jet around 30°S to the time it takes to reach the primary jet varies from 8 to 12 years. The time series shows that the largest anomalous activity occurs between 15°S and 20°S.

a. EOF Analysis

The spatial and temporal variability of the entire time series can be best quantified by the use of empirical orthogonal functions (EOFs) as shown in Fig. 3. The data were weighted to account for the decrease in area around latitude circles toward the pole, but were not weighted to account for the varying vertical layer depths. This shall not be important as we are mostly interested in the horizontal variations of the zonal flow. Using the North et al. (1982) test, the first and second EOFs are-well separated.

EOF1 shows an "equivalent barotropic" structure with maximum absolute anomalies at 19°S and 14°S. The black line represents the time-averaged location of the primary jet's maximum value (17.2°S). By comparing the mode's spatial structure and the mean location of

the jet, EOF1 describes meridional fluctuations of the main jet, or in other words, it captures the jet "wobbling" in the north-south direction (cf. annular modes.) This mode constitutes the largest amount (39.5 percent) of the total variability. In EOF2, the maximum anomalies are almost coincident with the mean location of the jet. Therefore, this mode indicates the intensifying and weakening of the main jet.

The spatial variability near the primary jet is analogous to the atmospheric annular modes, where the leading mode describes the zonal jet "wobbling," while the second mode captures its enhancement (e.g. Lorenz and Hartmann 2001). In our study, with EOF2 accounting for two-thirds as much variance as EOF1, this ratio is much larger than the atmospheric annular modes found by Lorenz and Hartmann (2001). This discrepancy is mainly attributed to the migrating jets. Unlike the atmosphere, there is an obvious non-dipole structure in both modes; as a result of the secondary jets, poleward of 20°S, three to four more additional extrema are present. Since successive EOFs are in quadrature with the first EOF, the local extrema for both modes are needed and must be of approximate equal importance in order to describe the migration of the zonal flow anomalies.

These leading modes of variability are robust. A similar spatial pattern develops after splitting the 313 years into different temporal segments (not shown). To illustrate how well the leading two modes capture both the spatial and temporal variability, we reconstruct the zonal flow by using the time-mean and just the first two eigenvectors. As seen in Fig. 4, not only do the secondary jets migrate equatorward, but also the primary jet oscillates laterally from its time-mean position. Therefore, the first two EOFs describes sufficiently

the variability (compare Fig. 1 with Fig. 4).

b. Description of EOF phases

The principal component captures the temporal variations associated with the spatial pattern of the EOFs. For instance, when the primary jet is displaced poleward (equatorward), the principal component associated with EOF1, PC1, will be positive (negative). Similarly, when the zonal flow at the primary jet is anomalously positive (negative), the principal component associated with EOF2, PC2, will be positive (negative).

Now that we have established how well the variability in the zonal average of $u(y, z, t)$ is represented by the two EOFs, we define the following four phases (shown in Table 1) to capture both the temporal and spatial variability. For instance, we define Phase A as PC1$<$0 and PC2$<$0, Phase B as PC1$<$0, PC2$>$0. A graphical representation of the four phases is shown in Fig. 5, as well as an example of a twenty-one year time series in the PC space. Throughout the 313-year time series, there is a sense of generally clockwise rotation, such that the following sequence occurs: Phase A $\rightarrow$ Phase B $\rightarrow$ Phase C $\rightarrow$ Phase D and then repeats back to Phase A. Since the secondary jets migrate, the principal components of both modes need to change sign to allow the secondary jets to advance equatorward and hence, this sequence is ultimately dictated by the behavior of the secondary jets.

Now that we have defined these four phases of the oscillation, we can thus describe the evolution of the structure of the zonal mean state as well as eddy fluxes by compositing all years associated with each phase. An example, which will be discussed in greater detail later,

is shown in Fig. 6. The sequence shows the primary jet wobbles, while the secondary jets migrate equatorward, precisely the behavior shown in Fig. 1. We can think of this sequence as a typical eight year cycle with each phase representing roughly two years.

Table 2 shows how closely the sequence was followed. Each change in phase is followed by the correct phase at least sixty-four percent of the time, e.g. the conditions prior to the onset of Phase A were correctly described to be in Phase D sixty-four percent of the time and incorrectly by Phase B or C thirty-six percent of the time. Similarly, Phase A described the PC space prior to Phase B eighty-five percent of the time. This shows that these pre-conditions are not symmetric, e.g. there is a stronger relation between Phase A and Phase B than there is between Phase D and Phase A. Our last statistical result worth mentioning, but will not be discussed further, brings attention to the duration of each phase. For our 313-year model study, Phase A constituted 95 years in total, nearly twenty percent more than any other phase. This behavior of the low zonal index occurring for longer durations appears consistent with the study done by Feldstein and Lee (1996), who examined the zonal index of the atmospheric jet in an aquaplanet.

4 Eddy Properties

a. Eddy-Mean Flow Interaction

Zonal flow anomalies shown in Fig. 2 are observed to persist on time scales that are larger than the frictional timescale associated with the bottom drag. Therefore, the anomalous

activity must be maintained by some forcing. The forcing likely responsible arises through eddy-mean flow interaction.

Following Edmon et al. (1980), we use the transformed Eulerian mean equation:

$$\frac{\partial[u]}{\partial t} - f[\widetilde{v}^*] = \nabla \cdot \vec{F} + D \tag{1}$$

where

$$\vec{F} = \Big(- a\cos\phi[u'v'], a\cos\phi f\frac{[v'T']}{[T_z]}\Big) \tag{2}$$

is the Eliassen-Palm (EP) flux vector (e.g. Edmon et al. 1980), D represents dissipation effects, $\widetilde{v}^*$ represents the motion necessary to conserve mass in the residual mean meridional circulation and square brackets represent zonal averages.

Fig. 6 shows the EP fluxes for each phase, as described in section 3. In all cases, equatorward of 12°S, where the isopycnals are relatively flat, little to no eddy activity is observed.

However, eddies are ubiquitous poleward of 12°S. In all EOF phases, the wave activity flux is upward; near the primary jet, the strongest flux occurs in Phase D and the weakest in Phase B. Comparing the different phases, both the eddy heat flux and eddy momentum flux are more dominant in the high zonal index (Phase C and D) than in the low zonal index (Phase A and B). Also, comparing the separate two zonal indexes, there is only a marginal difference in wave activity between the two high index phases (Phase C and Phase D) and similarly for the low index phases (Phase A and Phase B) . Put another way, consistent with EOF1 being the leading mode of zonal-mean zonal flow variability, the greatest change in

wave activity is associated with PC1.

We focus on anomalous EP flux vectors (i.e. departures from the time-mean) shown in Fig. 7. In this figure, anomalous baroclinic activity can be inferred by looking at the contoured zonal flow anomalies. Given the equivalent barotropic structure, an anomalously positive zonal flow implies enhanced baroclinicity, and thus enhanced baroclinic wavy activity. As the waves propagate away from this region, momentum gets transported towards the wave activity source (cf. Held and Andrews 1983).

Although the strongest horizontal eddy momentum flux (and its associated convergence) is at or near the jet, the maximum flow tendency does not occur there. As we will discuss in the next section, the divergence of the horizontal EP flux correlates much less with $\frac{\partial u}{\partial t}$ than with anomalous $[u]$, shown in Fig. 7.

b. Vertically-Integrated Momentum Budget

Since the jets are equivalent barotropic and we are more interested in how momentum gets redistributed latitudinally, we integrate the momentum budget across the entire depth. The Coriolis term vanishes, leaving only the horizontal component of the EP flux and friction:

$$\frac{\partial < [u] >}{\partial t} = -\left\langle \frac{\partial [u'v'] \cos^2 \phi}{a^2 \cos^2 \phi \partial \phi} \right\rangle + \tau_{surf} - \tau_{bot} \tag{3}$$

where vertically-integrated values are represented by angle brackets, τ_{surf} is the applied wind stress and τ_{bot} is the bottom wind stress. The first term on the right hand side (RHS) in the above equation will be referred to as the eddy forcing. Equation (3) demonstrates that the

vertically-integrated flow tendency is balanced by the vertically-integrated eddy forcing and the frictional effects.

A time-average of (3) is shown in Fig. 8a. When time-averaging, the flow tendency averages to zero and the only terms that contribute are on the RHS. To a first-order approximation, the wind stress is inputting momentum into the fluid and being removed by the bottom drag. However, near the primary jet, Reynolds' stresses contribute significantly; as shown in Fig. 8b, the eddy momentum flux converges at the jet.

Since we are interested in the anomalous activity, the annually-averaged, vertically-integrated anomalous momentum budget for each phase is plotted in Fig. 9. Since the applied wind stress is constant in time, this term does not contribute to the anomalous budget. As shown, there is a quasi-steady balance between the eddy forcing and friction. Flow tendency, being about ten percent of the terms on the RHS of (3) is essentially a residual. Consistent with the equatorward migrating zonal flow anomalies, the local maximum (minimum) flow tendency lies on the equatorward side of the maximum (minimum) zonal flow anomalies, which are denoted by dashed lines in Fig. 9.

Arguments in the next section will discuss how the divergence of the horizontal EP flux is asymmetric with respect to the zonal jets, in particular, they have larger values on the equatorward side. For example, in Phase A at 23°S, the peak of eddy forcing occurs on the equatorward side of the maximum positive zonal flow anomalies. This bias results in the flow tendency being larger on the equatorward side than its poleward counterpart, furthering the jet's equatorward migration. A similar argument holds for the equatorward migration of the

maximum negative zonal flow anomalies.

5 Discussion

Rossby waves on the sphere generally propagate equatorward (Edmon et al. 1980). From Chen and Robinson (1992), the refractive index for "equivalent barotropic" waves is as follows:

$$n^2 = \frac{\partial q}{\partial \phi} \frac{1}{([u] - (a\sigma cos\phi)/s)} - \frac{s^2}{a^2 cos^2 \phi} - \frac{f^2}{4N^2 H^2} \tag{4}$$

where a is the earth's radius, N^2 is the buoyancy frequency, σ is the wave frequency, q is the potential vorticity, and s is the spherical zonal wave number. From WKB theory, in regions of wave propagation, waves are refracted toward larger n^2. Because of the minus sign, each of the last two terms of (4) increase equatorward. Therefore, assuming if the latitudinal variations of the local PV gradient does not change significantly, there will be a tendency for the index of refraction to increase equatorward and thus, creating an equatorward bias in wave propagation.

The anomalous EP fluxes are directed out of the eastward zonal flow anomalies, and thus the momentum fluxes are directed into the secondary jets (cf. Held and Andrews 1983). However, as Fig. 10 shows, there is a bias whereby the magnitude of the fluxes is greater on the equatorward flank, and the flux convergence maximizes equatorward of the anomalous jet maxima. Thus, the secondary jets migrate equatorward.

We conclude this section by discussing why migrating jets were observed in this particular

study and not others (e.g. Panetta 1993). Even in this study, the primary jet did not migrate. So what causes some jets to migrate while others only "wobble?"

As we have discussed, the migration is a consequence of the equatorward bias in wave propagation. In quasi-geostrophic β-plane models, there are no spherical terms in the index of refraction, and hence no bias in the wave propagation. As a result, this may at least partially explain why jets do not migrate in such models (e.g. Panetta, 1993; Treguier and Panetta, 1994). However, primitive equation models which resolve the earth's curvature do not necessarily imply migrating jets as well. Although Lee (2005) may have modelled a hint of a weak equatorward migrating jet (see Fig. 3b in Lee 2005), for the most part, the multiple jets on a sphere only "wobbled."

Besides the spherical terms in the index of refraction, the PV gradient also affects wave propagation. It is important to point out that in the interior of the migrating jet region, PV is homogenized. While at the primary jet, there is a much larger interior PV gradient (cf. Cerovecki et al. (2006)) and, hence, the refractive index is greatly different than the secondary jets.

Along similar lines, since the local deformation radius is much smaller than the scale of the secondary jets, the direction of the eddy momentum flux is constantly upgradient. However, at the primary jet, with the deformation radius, L_D, larger, and a jet scale, L, $Bu \equiv \frac{L_D}{L} \sim 0.5$ (see Table 3.) From Held and Andrews (1983), this ratio of near one-half likely represents the transition region between upgradient and downgradient eddy momentum fluxes. Thus, the direction may no longer be consistent, and the eddy forcing may no longer

be near the jet axis.

6 Conclusion

As shown in Fig. 1, multiple zonal jets emerge when extremely broad buoyancy and wind forcing are applied. Although both forcings are constant in time, there is significant variability in the zonally-averaged zonal flow (see Fig. 2). Between 15°S and 20°S, a strong eastward jet oscillates meridionally, while between 20°S and 35°S, secondary (weaker) jets systematically migrate equatorward.

An EOF analysis describes the leading mode as an equivalent barotropic structure with the largest anomalies three degrees north and south of the primary jet's time-averaged position, similar to observed atmosphere (e.g. Thompson and Wallace 2000). However, unlike prior studies (e.g. Lorenz and Hartmann 2001), EOF2 accounts for more than two-thirds of what EOF1 captures in the total variability, a likely consequence of the migrating jets.

While precise necessary conditions for migrating jets remain elusive, some general constraints seem likely given our results. Firstly, the sphericity of the earth needs to be accounted. Secondly, as discussed in Panetta (1993), the width of the forcing needs to be extremely broad compared to the deformation radius to get multiple jets. Furthermore, by having the width of the baroclinically unstable region more than an order of magnitude greater than the jet scale, available potential energy away from the jet allow zonal flow anomalies to propagate. Finally, the jet scale needs to be much larger than the Rossby radius of deformation, in order for the direction of the eddy momentum fluxes to remain consistent

(cf. Held and Andrews 1983.)

7 Acknowledgements

This research was supported by the National Science Foundation under grants OCE-0426307 and ATM-0314094.

References

Cerovecki, I., R. A. Plumb, and W. Heres, 2006: Eddy transport and mixing in a wind and buoyancy driven jet on the sphere. *submitted to J. Phys. Oceanogr.*

Chen, P. and W. A. Robinson, 1992: Propagation of planetary waves between the troposphere and stratosphere. *J. Atmos. Sci.*, **49**, 2533–2545.

Cho, J. Y.-K. and L. M. Polvani, 1996: The emergence of jets and vorticies in freely evolving, shallow-water turbulence on a sphere. *Phys. Fluids*, **8**, 246–262.

Edmon, Jr., H. J., B. J. Hoskins, and M. E. McIntyre, 1980: Eliassen-Palm cross-sections for the troposphere. *J. Atmos. Sci.*, **37**, 2600–2615.

Feldstein, S., 1998: An observational study of the intraseasonal poleward propagation of zonal mean flow anomalies. *J. Atmos. Sci.*, **55**, 2516–2529.

Feldstein, S. and S. Lee, 1996: Mechanisms of zonal index variability in an aquaplanet GCM. *J. Atmos. Sci.*, **53**, 3541–3556.

Held, I. and D. G. Andrews, 1983: On the direction of the eddy momentum flux in baroclinic instability. *J. Atmos. Sci.*, **40**, 2220–2231.

Kuo, A., R. A. Plumb, and J. Marshall, 2005: Transformed Eulerian-mean theory. Part II: Potential vorticity homogenization and the equilibrium of a wind- and buoyancy-driven zonal flow. *J. Atmos. Sci.*, **35**, 157–187.

Lee, S., 2005: Baroclinic multiple zonal jets on the sphere. *J. Atmos. Sci.*, **62**, 2484–2498.

Lorenz, D. J. and D. L. Hartmann, 2001: Eddy-zonal flow feedback in the Southern Hemisphere. *J. Atmos. Sci.*, **58**, 3312–3327.

Marshall, J., A. Adcroft, C. Hill, L. Perelman, and C. Heisey, 1997: A finite-volume, incompressible Navier Stokes model for studies of the ocean on parallel computers. *J. Geophys. Res.*, **102**, 5753–5766.

Marshall, J., C. Hill, L. Perelman, and A. Adcroft, 1997: Hydrostatic, quasi-hydrostatic, and nonhydrostatic ocean modeling. *J. Geophys. Res.*, **102**, 5733–5752.

North, G. R., T. L. Bell, R. F. Cahalan, and F. J. Moeng, 1982: Sampling errors in the estimation of empirical orthogonal functions. **110**, 699–706.

Panetta, R. L., 1993: Zonal jets in wide baroclinically unstable regions: persistence and scale selection. *J. Atmos. Sci.*, **50**, 2073–2106.

Pater, I. and J. Lissauer, 2001: *Planetary Sciences.* Cambridge Univ. Press, 544 pp.

Rhines, P. B., 1975: Waves and turbulence on a beta-plane. *J. Fluid Mech.*, **69**, 417–443.

Rhines, P. B. and W. R. Young, 1982: Homogenisation of potential vorticity in planetary gyres. *J. Fluid Mech.*, **122**, 347–368.

Roden, G., 2000: Flow and water property structures beween the Bering Sea and Fiji in the summer of 1993. *J. Geophys. Res.*, **105**, 28,595–28612.

Thompson, D. W. J. and J. M. Wallace, 2000: Annular modes in the extratropical circulation. Part I: Month-to-month variability. *J. Climate*, **13**, 1000–1016.

Treguier, A. M. and R. L. Panetta, 1994: Multiple zonal jets in a quasigeostrophic model of the Antarctic circumpolar current. *J. Phys. Oceanogr.*, **24**, 2263–2277.

Williams, G., 1978: Planetary circulations: 1. Barotropic representation of Jovian and terrestrial turbulence. *J. Atmos. Sci.*, **35**, 1399–1426.

Williams, G. P., 2003: Jovian dynamics. Part III: Multiple, migrating, and equatorial jets. *J. Atmos. Sci.*, **60**, 1270–1296.

List of Figures

Figure 3 The leading two EOFs of the annually-averaged zonal-mean zonal flow. Solid (dashed) lines represent positive (negative) values. Black vertical line indicates position of the time-averaged jet. The percent variance is shown in the bottom right corner.

Figure 4 Time series of the reconstructed zonal flow using the leading two EOF modes.

Figure 5 The time series of the leading two principal components in PC space. The EOF phases are described in Table 1 are labelled in each quadrant. Each point is a one year average.

Figure 6 The total EP flux vectors for each EOF phase composite (labelled on bottom left corner) along with the zonally-averaged zonal flow.

Figure 7 Anomalous EP flux vectors for each EOF phase composite are plotted over the zonally-averaged zonal flow anomalies. Each phase is labelled at the bottom left corner of plot.

Figure 8 (a) Time-averaged quantities of the vertically-integrated zonal momentum budget. (b) Time-average of the vertically-integrated eddy momentum flux $< [u'v'] >$.

Figure 9 Terms to the vertically-integrated zonally-averaged anomalous momentum budget for each EOF phase. Vertically dashed lines correspond to maximum zonal flow anomalies.

Figure 10 Anomalous horizontal EP flux (line) for each EOF phase plotted over zonally-averaged zonal flow anomalies (in color).

List of Tables

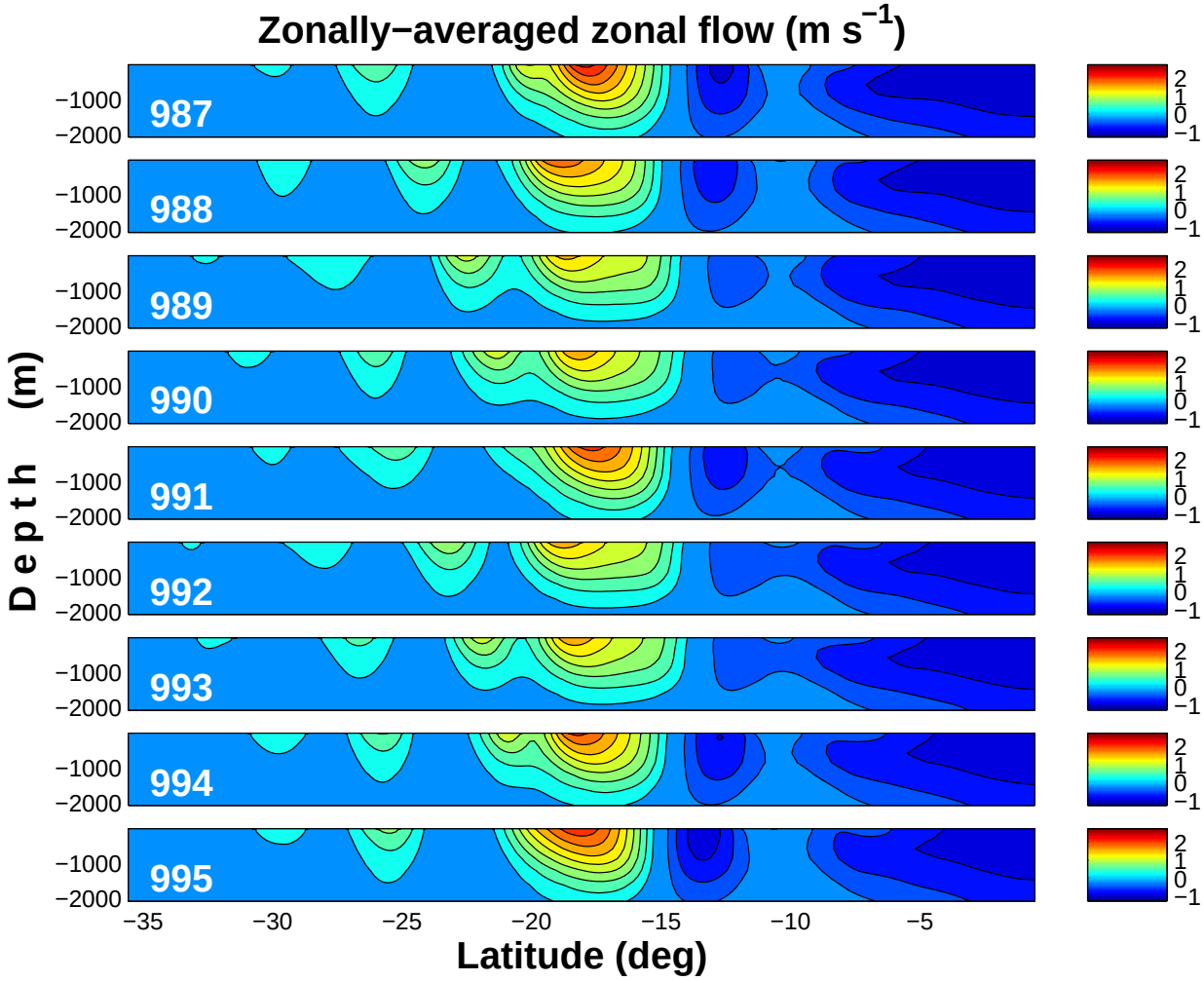

Figure 1: Time series of the annually-averaged zonally-averaged zonal flow. Time stamps (in years) are located on bottom left corner of each plot.

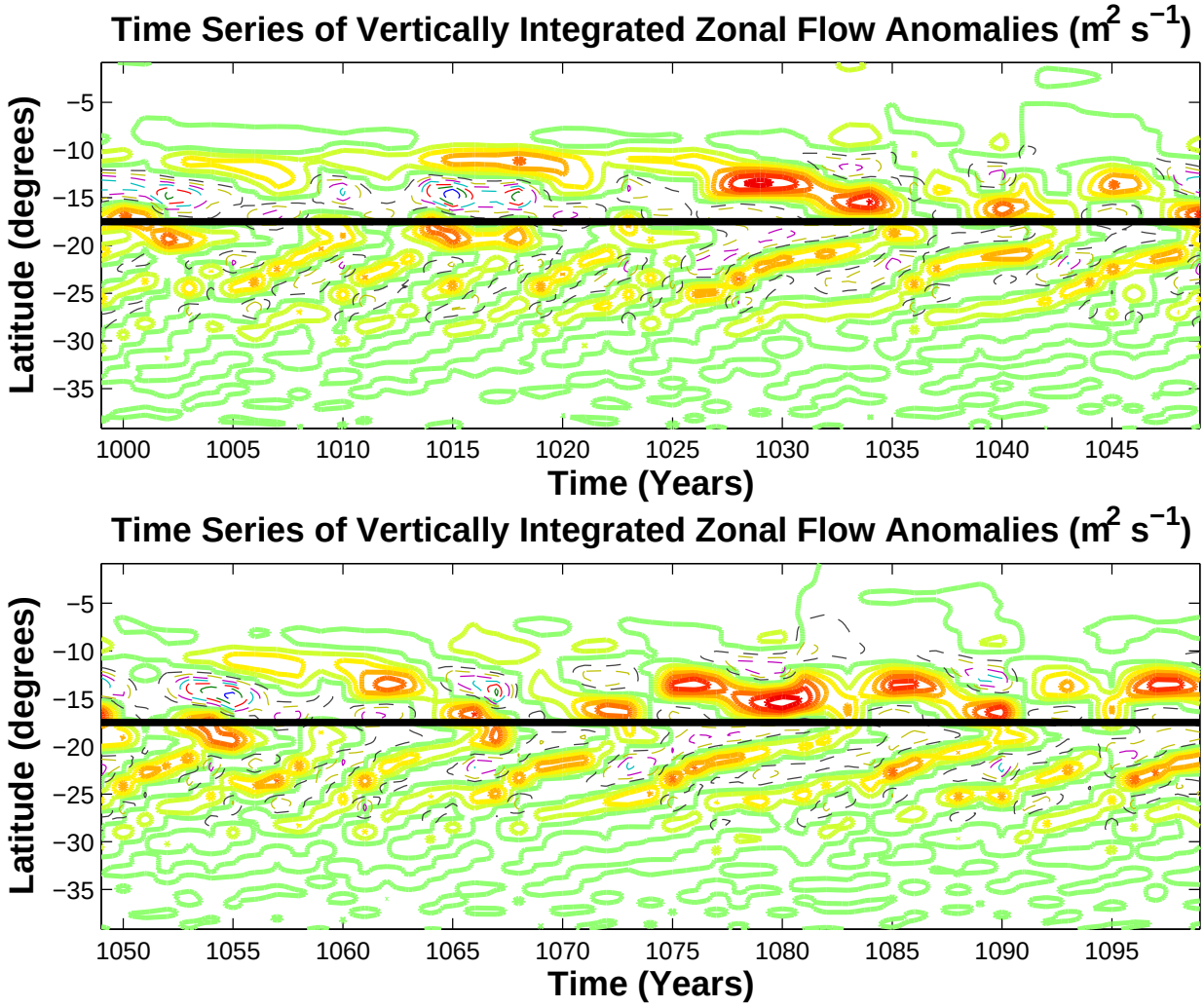

Figure 2: Time series of the anomalous vertically-integrated zonally-averaged zonal flow. Positive contours start at 20 and increase in increments of 200. Negative contours (dashed lines) start at -200 and are also in increments of 200.

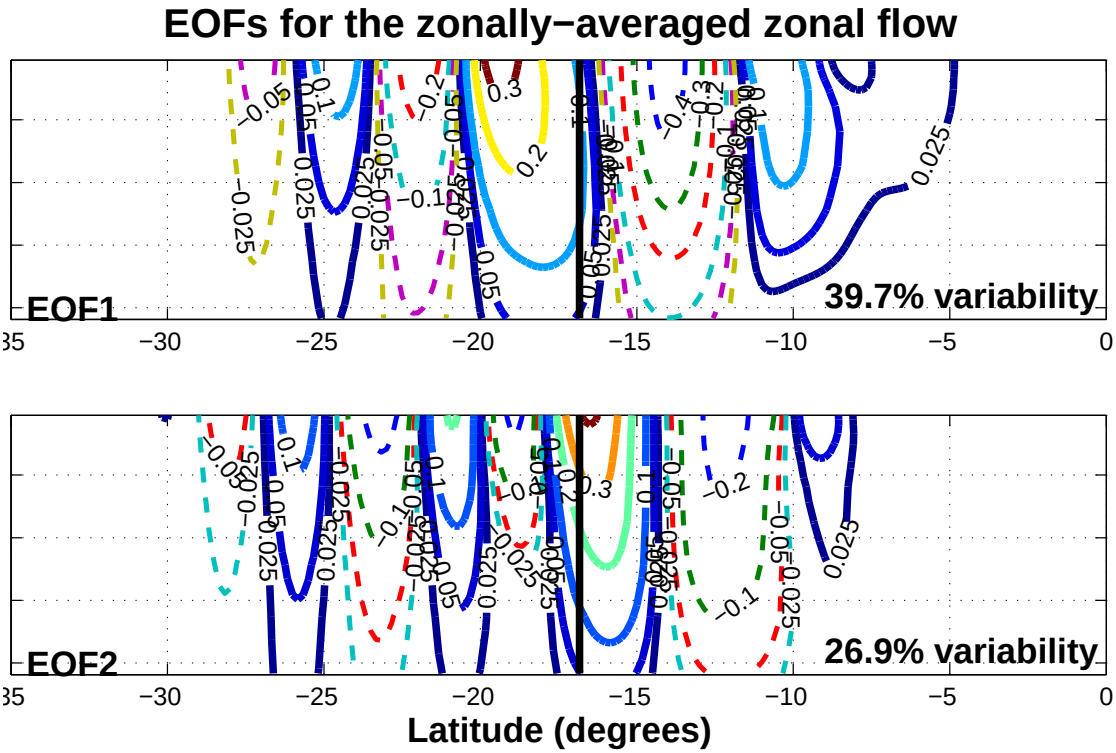

Figure 3: The leading two EOFs of the annually-averaged zonal-mean zonal flow. Solid (dashed) lines represent positive (negative) values. Black vertical line indicates position of the time-averaged jet. The percent variance is shown in the bottom right corner.

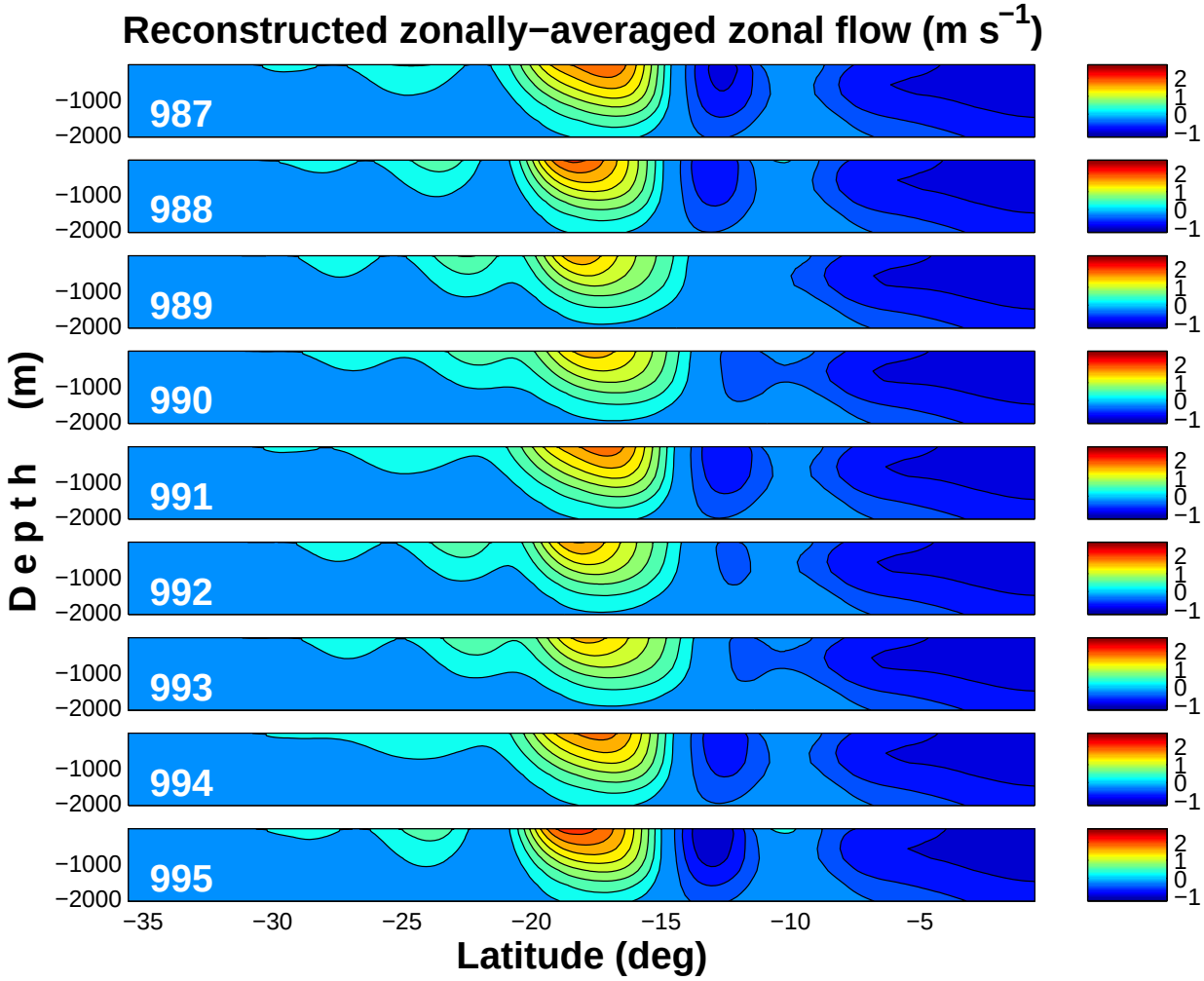

Figure 4: Time series of the reconstructed zonal flow using the leading two EOF modes.

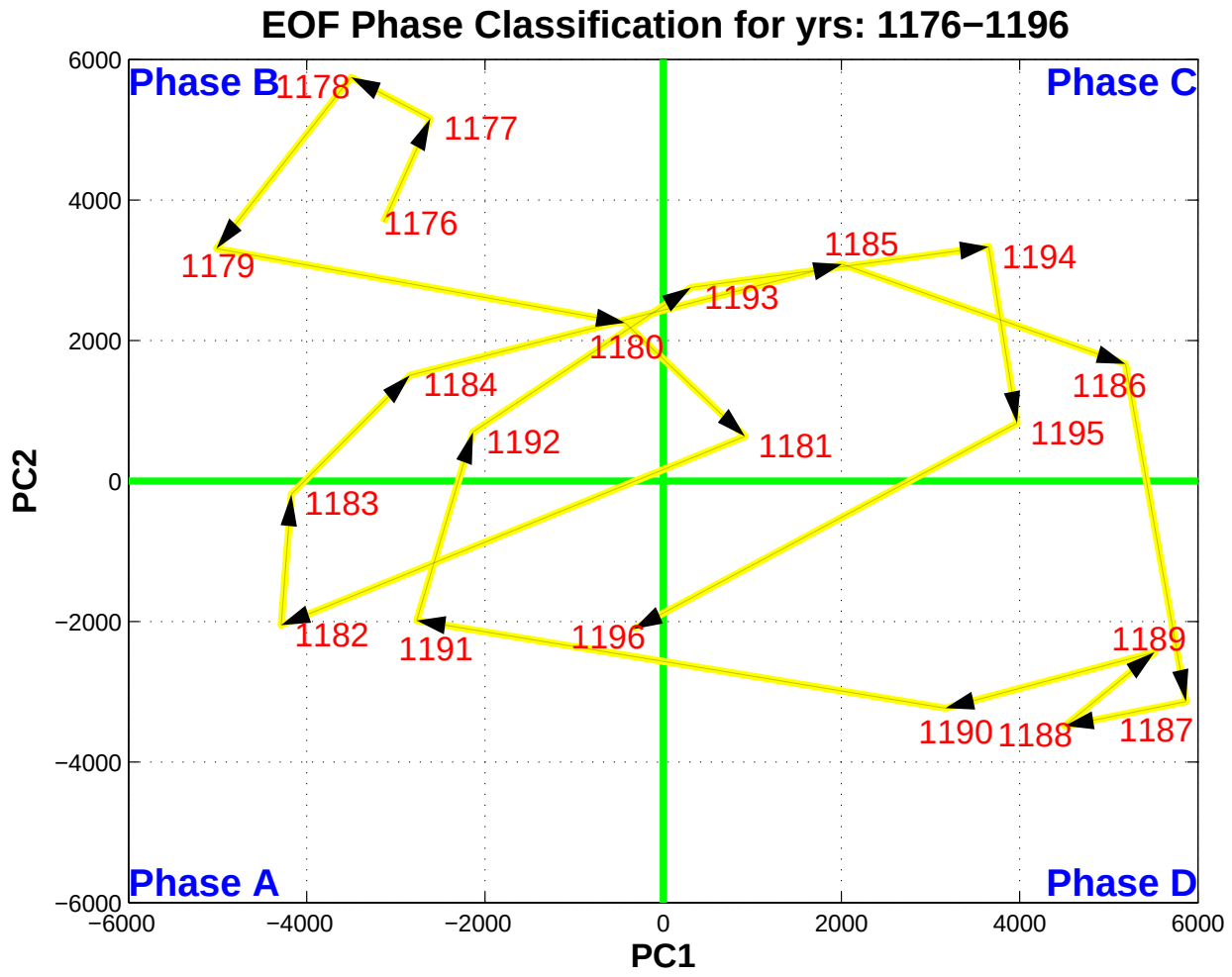

Figure 5: The time series of the leading two principal components in PC space. The EOF phases are described in Table 1 are labelled in each quadrant. Each point is a one year average.

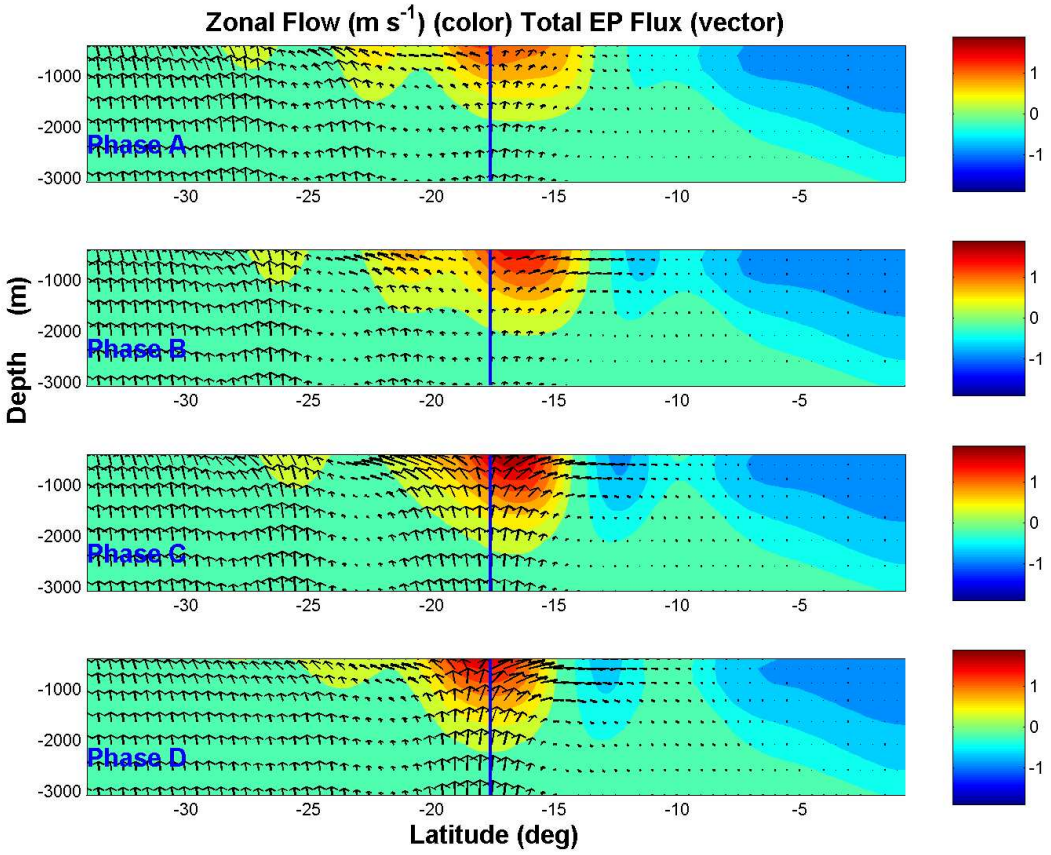

Figure 6: The total EP flux vectors for each EOF phase composite (labelled on bottom left corner) along with the zonally-averaged zonal flow.

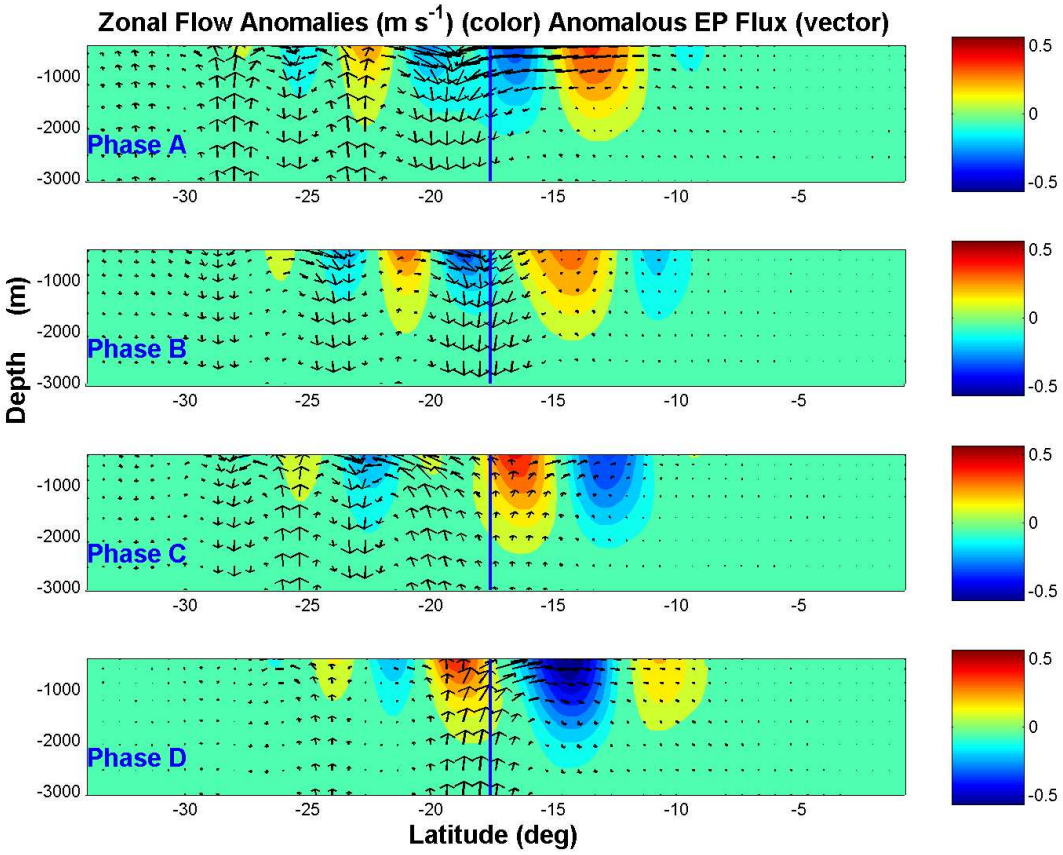

Figure 7: Anomalous EP flux vectors for each EOF phase composite are plotted over the zonally-averaged zonal flow anomalies. Each phase is labelled at the bottom left corner of plot.

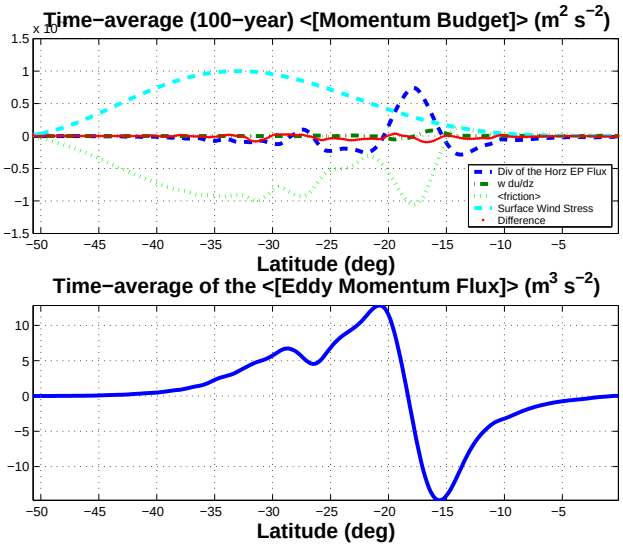

Figure 8: (a) Time-averaged quantities of the vertically-integrated zonal momentum budget. (b) Time-average of the vertically-integrated eddy momentum flux $< [u'v'] >$.

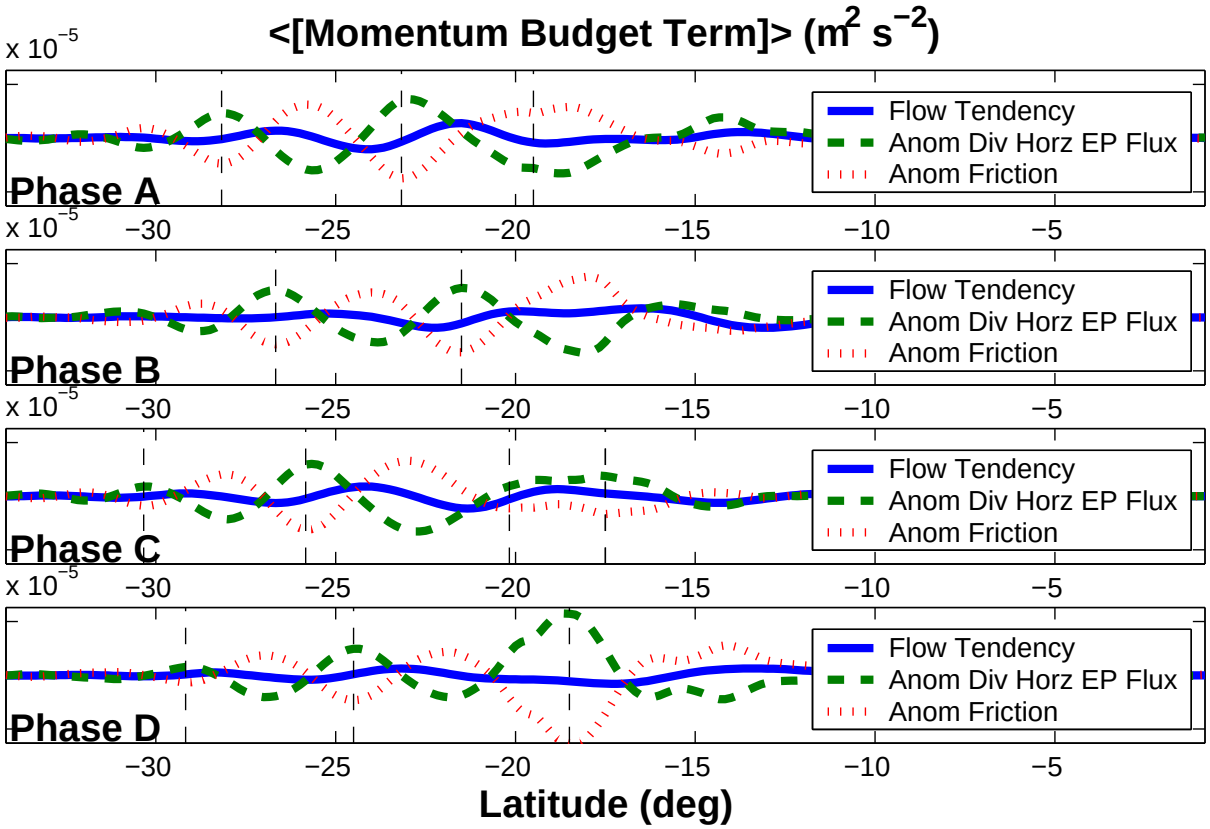

Figure 9: Terms to the vertically-integrated zonally-averaged anomalous momentum budget for each EOF phase. Vertically dashed lines correspond to maximum zonal flow anomalies.

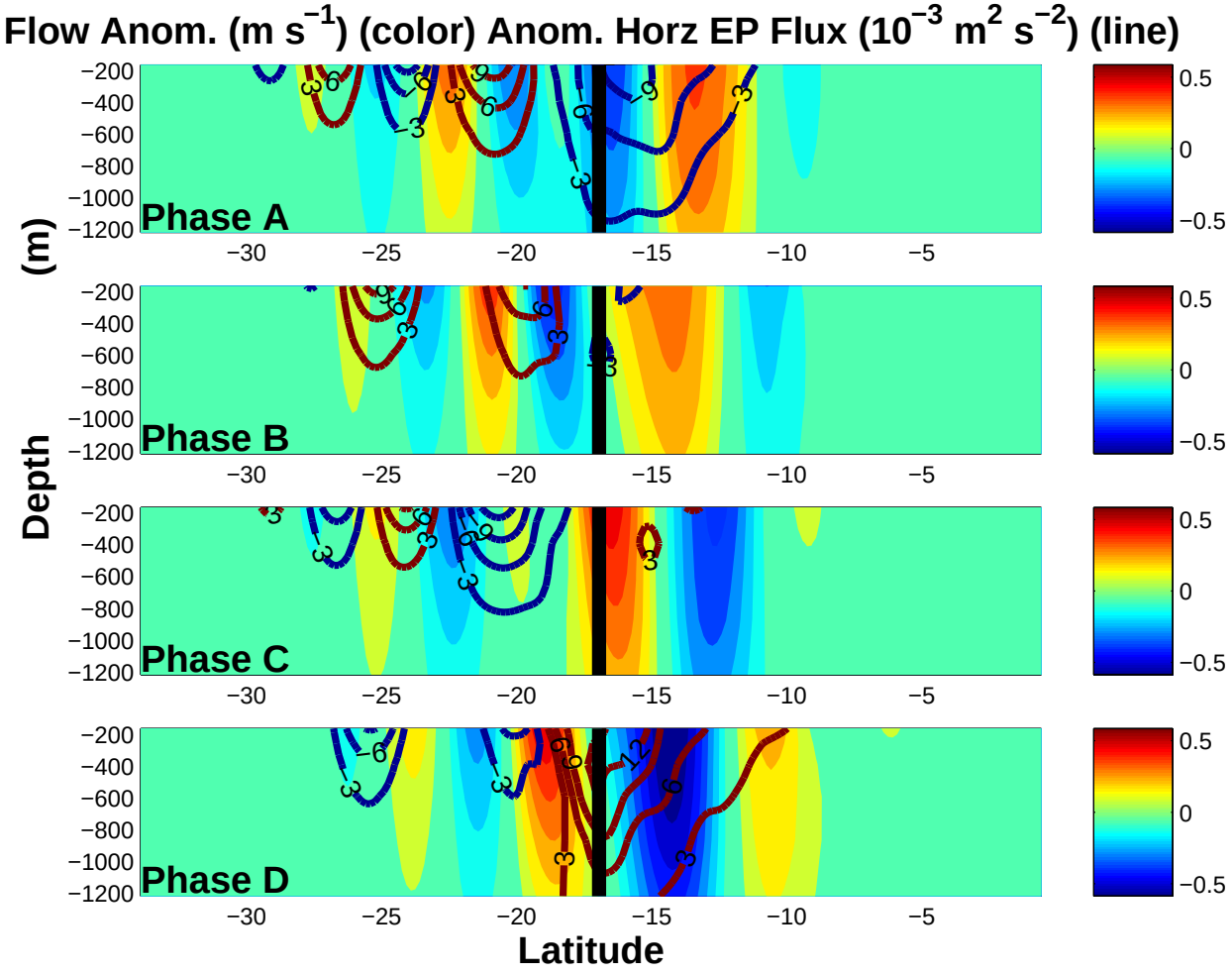

Figure 10: Anomalous horizontal EP flux (line) for each EOF phase plotted over zonally-averaged zonal flow anomalies (in color).

Table 1: Physical characteristics of the primary jet in the four EOF phases.

	Phase A	Phase B	Phase C	Phase D
PC1	Negative	Negative	Positive	Positive
PC2	Negative	Positive	Positive	Negative
Displacement	Equatorward	Equatorward	Poleward	Poleward
Strength	Decreasing	Increasing	Increasing	Decreasing

Table 2: Statistical results on the conditions prior to the onset of each phase and zonal index.

	Phase A	Phase B	Phase C	Phase D
Prior to Phase A	–	7%	29%	64%
Prior to Phase B	85%	–	15%	0%
Prior to Phase C	16%	79%	–	5%
Prior to Phase D	19%	6%	75%	–
Prior to High Zonal Index	26%	74%	–	–
Prior to Low Zonal Index	–	–	39%	61%

Table 3: The scales of the deformation radius (L_D) and the jet scales (L) in the separate regimes.

	L_D (km)	L (km)	$Bu \equiv \frac{L_D}{L}$
Migrating Region	10	100	0.1
"Wobbling" Region	200	400	0.5